Bayesian Analysis of the DAMPE Lepton Spectra and Two Simple Model Interpretations

Jia-Shu Niu,[1,2,*] Tianjun Li,[1,2,†] Ran Ding,[3] Bin Zhu,[4] Hui-Fang Xue,[5] and Yang Wang[6]

[1] *CAS Key Laboratory of Theoretical Physics, Institute of Theoretical Physics, Chinese Academy of Sciences, Beijing, 100190, China*

[2] *School of Physical Sciences, University of Chinese Academy of Sciences, No. 19A Yuquan Road, Beijing 100049, China*

[3] *Center for High-Energy Physics, Peking University, Beijing, 100871, P. R. China*

[4] *Department of Physics, Yantai University, Yantai 264005, P. R. China*

[5] *Astronomy Department, Beijing Normal University, Beijing 100875, P.R.China*

[6] *School of Mathematical Sciences, Shanxi University, Shanxi 030006, P.R. China.*

(Dated: December 4, 2017)

Recently, DAMPE has released its first results on the high-energy cosmic-ray electrons and positrons (CREs) from about 25 GeV to 4.6 TeV, which directly detect a break at ~ 1 TeV. This result gives us an excellent opportunity to study the source of the CREs excess. We first reproduce the proton, helium flux and $\bar{\mathrm{p}}/\mathrm{p}$ ratio data from AMS-02 and CREAM (above $\sim$ TeV) by global fitting (Step I), which determine not only the propagation parameters but also the primary source parameters of proton and helium spectra. With the best fitting parameters from Step I, we do global fitting on the CREs flux from DAMPE and positron flux from AMS-02 (Step II). In this step, we consider two separate scenarios (pulsar and dark matter annihilation via leptonic channels) to construct the bump ($\gtrsim 100$ GeV) and the break at ~ 1 TeV. The result shows: (i) in pulsar scenario, the spectral index of the injection should be $\nu_{psr} \sim 0.68$ and the cut-off should be $R_c \sim 660$ GV; (ii) in dark matter scenario, the dark matter particle's mass is $m_\chi \sim 1208$ GeV and the cross section is $\langle \sigma v \rangle \sim 1.48 \times 10^{-23}\,\mathrm{cm}^3\,\mathrm{s}^{-1}$. Moreover, in the dark matter scenario, the $\tau\bar{\tau}$ annihilation channel is highly suppressed. If we deduct the line spectral signal at ~ 1.4 TeV, the CREs data from DAMPE favors the dark matter interpretation. Although the source of the line spectral signal is different from the source of the smooth background in high confidence, this need the accumulation of the events and the updated data to confirm. Furthermore, we present two simple dark matter models to explain the DAMPE results by introducing an SM singlet scalar S as dark matter particle. In one model, we introduce a doublet scalar H' as a mediator, while in the other model we introduce a pair of vector-like fermions (XE, XE^c). In these models, the real scalar dark matter can annihilate dominantly into the charged lepton pairs.

arXiv:1712.00372v1 [astro-ph.HE] 30 Nov 2017

I. INTRODUCTION

Recently, DAMPE (DArk Matter Particle Explorer) [1] Satellite, which has been launched on December 17, 2015, has released its first data on high-energy cosmic-ray electrons and positrons (CREs)[2]. DAMPE has measured the CREs (i.e., $e^- + e^+$) spectrum in the range of 25 GeV − 4.6 TeV with unprecedented energy resolution (1.5% at 100 GeV). The results shows a bumps at about 100 GeV − 1 TeV which is consistent with previous results [3–8]. More interesting, a break at ~ 1 TeV and a line spectral signal at ~ 1.4 TeV have been detected. All of these features cannot be described by a single power law and provide us an opportunity to study the source of high-energy CREs.

In cosmic ray (CR) theory, the CR electrons are expected to be accelerated during the acceleration of CR nuclei at the sources, e.g. supernova remnants (SNRs). But the CR positrons are produced as secondary particles from CR nuclei interaction with the interstellar medium (ISM) [3, 9–11]. From the results of the flux of positrons and electrons [5, 12–14], we can infer that there should be some extra sources producing electron-positron pairs. This can be interpreted both by the astrophysical sources' injection [15–22] and dark matter (DM) annihilation or decay [23–28].

As a result, the CREs data contains the primary electrons, the secondary electrons, the secondary positrons and the extra source of electron-positron pairs. If we want to study the properties of the extra source, we should deduct the primary electrons and secondary electrons/positrons first. The primary electrons are always assumed to have a power-law form injection and the secondary electrons/positrons are determined dominatingly by the CR proton and helium particles interact with ISM. Consequently, we should do global fitting to these data simultaneously.

Considering the situations of high-dimentional parameter space of propagation model and precise data sets, we employ a Markov Chain Monte Carlo (MCMC [29]) method (embed by DRAGON) to do global fitting and sample the parameter space of CR propagation and nuclei injections [30–33]. The lepton data was fitted by using background (including the primary electrons and secondary electrons/positrons) and extra sources (the pulsar and DM scenario) simultaneously, which can avoid the bias of choosing the lepton background parameters.

* jsniu@itp.ac.cn

† tli@itp.ac.cn

Moreover, because of the significant difference in the slopes of proton and helium, of about ~ 0.1 [34–38], has been observed, we use separate primary source spectra settings for proton and helium. Note also that we consider propagation of nuclei only up to $Z = 2$ and neglect possible contributions from the fragmentation of $Z > 2$ nuclei, which should be a good approximation since their fluxes are much lower than the p and He fluxes [39]. In this condition, all the secondary particles (antiprotons and leptons) are produced from the interactions between proton, helium and ISM, which give us a self-consistent way to combine the nuclei and lepton data together.

Although the electron energy range covered by AMS-02 is under TeV and there are systematics between the AMS-02 and DAMPE CREs data, fittings to the AMS-02 leptonic data provide a self-consistent picture for the extra source models. As the extra sources accounting for the AMS-02 results may provide contribution to the TeV scale, the AMS-02 data could also constrain the properties of the predicted $e^- + e^+$ spectrum above $\sim$ TeV. Considering the degeneracy between the different lepton data, we use the positron flux from AMS-02 and CREs flux from DAMPE together to constraint the extra source properties. The systematics are dealt with by employing a re-scale factor c_{e^+} on positron flux.

Furthermore, we propose two simple models to explain the DAMPE results. In these models, we introduce an SM singlet scalar S. We assume that S is odd under a discrete Z_2 symmetry and then a dark matter candidate. In Model I, we introduce a doublet scalar H' without a Vacuum Expectation Value (VEV) or with a very small VEV. and H' couples dominantly to the charged leptons. With the term S^2HH' where H is the SM Higgs field, the dark matter particles can annihilate dominantly into charged leptons via s channel after electroweak symmetry breaking. In Model II, we introduce a pair of vector-like fermions (XE, XE^c), which are odd under Z_2 symmetry as well. Thus, the dark matter particles can annihilate into charged leptons via t and u channels.

This paper is organized as follows. We first introduce the theory of propagation of CRs in the Galaxy and the corresponding configurations of our work in Sec. II. The global fitting method and the chosen data sets and parameters is give in Sec. III. After present the fitting results and add some discussions in Sec. IV. We present our model in Sec. V, and summarize our results in Sec. V.

II. SETUPS

A. Propagation model

Galactic CR particles diffuse in the Galaxy after being accelerated, experiencing the fragmentation and energy loss in the ISM and/or the interstellar radiation field (ISRF) and magnetic field, as well as decay and possible reacceleration or convection. Denoting the density of CRs per unit momentum interval as ψ (which is related to the phase space density $f(\mathbf{r}, \mathbf{p}, t)$ as $\psi(\mathbf{r}, p, t) = 4\pi p^2 f(\mathbf{r}, \mathbf{p}, t)$), the propagation can be described by the propagation equation [40]

$$\frac{\partial \psi}{\partial t} = Q(\mathbf{r}, p) + \nabla \cdot (D_{xx} \nabla \psi - \mathbf{V}_c \psi) + \frac{\partial}{\partial p} p^2 D_{pp} \frac{\partial}{\partial p} \frac{1}{p^2} \psi - \frac{\partial}{\partial p} \left[\dot{p} \psi - \frac{p}{3} (\nabla \cdot \mathbf{V}_c \psi) \right] - \frac{\psi}{\tau_f} - \frac{\psi}{\tau_r}, \quad (1)$$

where $Q(\mathbf{r}, p)$ is the source distribution, D_{xx} is the spatial diffusion coefficient, $\mathbf{V}_c$ is the convection velocity, D_{pp} is diffusion coefficient in the momentum-space, τ_f and τ_r are the characteristic time scales used to describe the fragmentation and radioactive decay.

The convection velocity $\mathbf{V}_c$ is generally assumed to linearly depend on the distance away from the Galaxy disk, $\mathbf{V}_c = \mathbf{z} \cdot \mathrm{d}V_c / \mathrm{d}z$, where $\mathbf{z}$ is the position vector in the vertical direction to the galactic disk. Such a configuration can avoid the discontinuity at the galactic plane. In this work, we did not consider the effect of convection which is disfavored by the AMS-02 nuclei data [33].

The diffusion coefficient can be parameterized as

$$D_{xx} = D_0 \beta \left(R/R_0 \right)^{\delta} \ , \quad (2)$$

where β is the velocity of the particle in unit of light speed c, R_0 is the reference rigidity, and $R \equiv pc/Ze$ is the rigidity.

The reacceleration effect is always used to describe with the diffusion in momentum space. Considering the scenario in which the CR particles are reaccelerated by colliding with the interstellar random weak hydrodynamic waves, the relation between the spatial diffusion coefficient D_{xx} and the momentum diffusion coefficient D_{pp} can be expressed as [41]

$$D_{pp} D_{xx} = \frac{4 p^2 v_A^2}{3\delta(4-\delta^2)(4-\delta)\omega}, \quad (3)$$

where v_A is the Alfven velocity and the parameter ω is used to characterize the level of the interstellar turbulence. Because only v_A^2/ω plays a role, we adopt $\omega = 1$ and use v_A to characterize the reacceleration. Free escape is assumed at boundaries, r_h and z_h, for the cylindrical coordinate system.

High energy leptons (electrons or positrons) loss energy due to the processes like inverse Compton scattering and synchrotron radiation. The typical propagation length is around a few kpc for lepton energy around 100 GeV. In the calculation of energy loss rate, the interstellar magnetic field in cylinder coordinates (r, z) is assumed to have the form

$$B(r, z) = B_0 \exp\left(-\frac{r - r_\odot}{r_B} \right) \exp\left(-\frac{|z|}{z_B} \right), \quad (4)$$

where $B_0 = 5 \times 10^{-10}$ Tesla, $r_B = 10$ kpc, $z_B = 2$ kpc [42], and $r_\odot \approx 8.5$ kpc is the distance from the Sun to the galactic center.

In this work, we use the diffusion-reacceleration model which is widely used and can give a consistent fitting results to the AMS-02 nuclei data (see for e.g., Niu and Li [33]).

B. Sources

1. Primary sources

The injection spectra of all kinds of nuclei are assumed to be a broken power law form

$$q_{\rm i}(p) = N_{\rm i} \times \begin{cases} \left(\dfrac{R}{R_{\rm A}}\right)^{-\nu_{\rm A1}} & R \le R_{\rm A} \\ \left(\dfrac{R}{R_{\rm A}}\right)^{-\nu_{\rm A2}} & R > R_{\rm A} \end{cases}, \tag{5}$$

where i denotes the species of nuclei, $N_{\rm i}$ is the normalization constant proportional to the relative abundance of the corresponding nuclei, and $\nu_{\rm A} = \nu_{\rm A1}(\nu_{\rm A2})$ for the nucleus rigidity R below (above) a reference rigidity $R_{\rm A}$.

In this work, considering the fine structure of spectral hardening for primary nuclei at $\sim 300\,$GV (which was observed by ATIC-2 [34], CREAM [35], PAMELA [36], and AMS-02 [37, 38]) and the observed significant difference in the slopes of proton and helium (of about ~ 0.1 [37, 38, 43]), we use separate primary source spectra settings for proton and helium and each of them has 2 breaks at rigidity $R_{\rm A1}$ and $R_{\rm A2}$. The corresponding slopes are $\nu_{\rm A1}$ ($R \le R_{\rm A1}$), $\nu_{\rm A2}$ ($R_{\rm A1} < R \le R_{\rm A2}$) and $\nu_{\rm A3}$ ($R > R_{\rm A3}$). For cosmic-ray electrons primary source, we followed the same configuration as proton and helium. But due to the DAMPE lepton data range ($20\,$GeV$-4\,$TeV), we use 1 break R_e for electron primary source, and the corresponding slopes are ν_{e1} ($R \le R_e$) and ν_{e2} (($R > R_e$)).

The radial distribution of the source term can be determined by independent observables. Based on the distribution of SNR, the spatial distribution of the primary sources is assumed to have the following form [44]

$$f(r,z) = q_0 \left(\frac{r}{r_\odot}\right)^a \exp\left[-b \cdot \frac{r - r_\odot}{r_\odot} - \frac{|z|}{|z_s|}\right], \tag{6}$$

where $a = 1.25$ and $b = 3.56$ are adapted to reproduce the Fermi-LAT gamma-ray data of the 2nd Galactic quadrant [45–47], $z_s \approx 0.2$ kpc is the characteristic height of Galactic disk, and q_0 is a normalization parameter. In the 2D diffusion model, one can use the realistic non-uniform interstellar gas distribution of $H_{\rm I,II}$ and H_2 determined from 21cm and CO surveys. Thus, the injection source function for a specific CR species can be written as follows

$$Q(\mathbf{r}, p) = f(r,z) \cdot q_i(p). \tag{7}$$

2. Secondary sources

The secondary cosmic-ray particles are produced in collisions of primary cosmic-ray particles with ISM. The secondary antiprotons are generated dominantly from inelastic pp-collisions and pHe-collisions. At the same time, the secondary electrons and positrons are the final product of decay of charged pions and kaons which in turn mainly created in collisions of primary particles with gas. As a result, the corresponding source term of secondary particles can be expressed as

$$q_{\rm sec} = \frac{c}{4\pi} \sum_{i={\rm H,He}} n_i \sum_j \int {\rm d}p' \beta n_j(p') \frac{{\rm d}\sigma_{i,j}(p,p')}{{\rm d}p} \tag{8}$$

where n_i is the number density of interstellar hydrogen (helium), ${\rm d}\sigma_{i,j}(p,p')/{\rm d}p$ is the differential production cross section, $n_j(p')$ is the CR species density and p' is the total momentum of a particle.

To partially take into account the uncertainties when calculating the secondary fluxes, we employ a parameter $c_{\bar{\rm p}}$ and c_{e^+} to re-scale the calculated secondary flux to fit the data [31, 48–51]. Note that the above mentioned uncertainties may not be simply represented with a constant factor, but most probably they are energy dependent [52, 53]. Here we expect that a constant factor is a simple assumption.

3. Extra sources

The primary source term of CR particles from the annihilation of Majorana DM particles has the form

$$Q(\boldsymbol{r}, p) = \frac{\rho(\boldsymbol{r})^2}{2m_\chi^2} \langle \sigma v \rangle \sum_f \eta_f \frac{dN^{(f)}}{dp}, \tag{9}$$

where $\langle \sigma v \rangle$ is the velocity-averaged DM annihilation cross section multiplied by DM relative velocity (referred to as cross section) which is the quantity appears in the Boltzmann equation for calculating the evolution of DM number density. $\rho(\boldsymbol{r})$ is the DM energy density distribution function, and $dN^{(f)}/dp$ is the injection energy spectrum of electrons (positrons) from DM annihilating into standard model (SM) final states through all possible intermediate states f with η_f the corresponding branching fractions. In this work, we considered DM annihilation via leptonic channels, the corresponding branching fractions for e^-e^+, $\mu\bar{\mu}$, and $\tau\bar{\tau}$ are η_e, η_μ, and η_τ respectively ($\eta_e + \eta_\mu + \eta_\tau = 1$).

We use the results of PPPC 4 DM ID [54], which includes the electroweak corrections [55], to calculate the electron (positron) spectrum from DM annihilation by different channels.

The fluxes of cosmic-ray particles from DM annihilation depend also on the choice of DM halo profile, which we here employ the Einasto profile [56–59]:

$$\rho(r) = \rho_\odot \exp\left[-\left(\frac{2}{\alpha}\right)\left(\frac{r^\alpha - r_\odot^\alpha}{r_s^\alpha}\right)\right], \tag{10}$$

with $\alpha \approx 0.17$, $r_s \approx 20\,\mathrm{kpc}$ and $\rho_\odot \approx 0.39\,\mathrm{GeV\,cm^{-3}}$ is the local DM energy density [60–64].

The pulsars as an extra source will also be considered in this work, which are able to generate high energy positron-electron pairs through the electromagnetic cascade in the magnetic pole region. The injection spectrum of the electrons and positrons is usually assumed to be a power law with an exponential cutoff

$$q_e^{\rm psr}(p) = N_{\rm psr}(R/1\,\mathrm{GeV})^{-\nu_{\rm psr}} \exp\left(-R/R_{\rm c}\right), \qquad (11)$$

where $N_{\rm psr}$ is the normalization factor, $\nu_{\rm psr}$ is the spectral index, $R_{\rm c}$ is the cutoff rigidity. We adopt a continuous and stable pulsar injection. The spatial distribution obeys the same form of Eq. (6), with slightly different parameters $a = 2.35$ and $b = 5.56$ [31].

C. Solar modulation

The interstellar flux of the cosmic-ray particle is related to its density function as

$$\Phi = \frac{v}{4\pi}\psi(\boldsymbol{r}, p)\ . \qquad (12)$$

For high energy nuclei $v \approx c$. We adopt the force-field approximation [65] to describe the effects of solar wind and helioshperic magnetic field in the solar system, which contains only one parameter the so-called solar-modulation ϕ. In this approach, the cosmic-ray nuclei flux at the top of the atmosphere of the Earth which is observed by the experiments $\Phi_{\rm obs}$ is related to the interstellar flux as follows

$$\Phi_{\rm obs}(E_{\rm obs}) = \left(\frac{2mE_{\rm obs} + E_{\rm obs}^2}{2mE_{\rm kin} + E_{\rm kin}^2}\right)\Phi(E_{\rm kin}), \qquad (13)$$

where $E_{\rm obs} = E_{\rm kin} - |Z|e\phi$ is the kinetic energy of the cosmic-ray nuclei measured by the experiments, where Z is the charge number of the cosmic ray particles.

Considering the charge-sign dependence solar modulation represented in the previous fitting [33], we use $\phi_{\rm nuc}$ for nuclei (proton and helium) data and $\phi_{\bar{\rm p}}$ for $\bar{\rm p}$ data to do the solar modulation. At the same time, we use ϕ_{e^+} to modulate the positron flux. Because the DAMPE lepton data $\gtrsim 20\,\mathrm{GeV}$, we did not consider the modulation effects on electrons (or leptons).

D. Numerical tools

The public code DRAGON [1] [66] was used to solve the diffusion equation of Eq. (1) numerically, because its better performance on clusters. Some custom modifications are performed in the original code, such as the possibility to use specie-dependent injection spectra, which is not allowed by default in DRAGON.

In view of some discrepancies when fitting with the new data which use the default abundance in DRAGON [67], we use a factor $c_{\rm He}$ to rescale the helium-4 abundance (which has a default value of 7.199×10^4) which help us to get a global best fitting.

The radial and z grid steps are chosen as $\Delta r = 1\,\mathrm{kpc}$, and $\Delta z = 0.5\,\mathrm{kpc}$. The grid in kinetic energy per nucleon is logarithmic between $0.1\,\mathrm{GeV}$ and $220\,\mathrm{TeV}$ with a step factor of 1.2. The free escape boundary conditions are used by imposing ψ equal to zero outside the region sampled by the grid.

III. FITTING PROCEDURE

A. Bayesian Inference

In this work, we use Bayesian inference to get the posterior probability distribution function (PDF), which is based on the following formula

$$p(\boldsymbol{\theta}|D) = \frac{\mathcal{L}(D|\boldsymbol{\theta})\pi(\boldsymbol{\theta})}{p(D)}, \qquad (14)$$

where $\boldsymbol{\theta} = \{\theta_1, \ldots, \theta_m\}$ is the free parameter set, D is the experimental data set, $\mathcal{L}(D|\boldsymbol{\theta})$ is the likelihood function, and $\pi(\boldsymbol{\theta})$ is the prior PDF which represents our state of knowledge on the values of the parameters before taking into account of the new data. (The quantity $p(D)$ is the Bayesian evidence which is not that important in this work but it is important for Bayesian model comparison.)

We take the prior PDF as a uniform distribution

$$\pi(\theta_i) \propto \begin{cases} 1, \text{ for } \ \theta_{i,\min} < \theta_i < \theta_{i,\max} \\ 0, \text{ otherwise} \end{cases}, \qquad (15)$$

and the likelihood function as a Gaussian form

$$\mathcal{L}(D|\boldsymbol{\theta}) = \prod_i \frac{1}{\sqrt{2\pi\sigma_i^2}} \exp\left[-\frac{(f_{{\rm th},i}(\boldsymbol{\theta}) - f_{{\rm exp},i})^2}{2\sigma_i^2}\right], \qquad (16)$$

where $f_{{\rm th},i}(\boldsymbol{\theta})$ is the predicted i-th observable from the model which depends on the parameter set $\boldsymbol{\theta}$, and $f_{{\rm exp},i}$ is the one measured by the experiment with uncertainty σ_i.

Here we use the algorithms such as the one by Goodman and Weare [68] instead of classical Metropolis-Hastings for its excellent performance on clusters. The algorithm by Goodman and Weare [68] was slightly altered and implemented as the Python module `emcee`[2] by Foreman-Mackey et al. [69], which makes it easy to use

[1] https://github.com/cosmicrays/DRAGON

[2] http://dan.iel.fm/emcee/

by the advantages of Python. Moreover, `emcee` could distribute the sampling on the multiple nodes of modern cluster or cloud computing environments, and then increase the sampling efficiency observably.

B. Data Sets and Parameters

In our work, we first use the MCMC method to reproduce the proton (from AMS-02 and CREAM [35, 37]), helium (from AMS-02 and CREAM [35, 38]) and $\bar{\mathrm{p}}/\mathrm{p}$ (from AMS-02 [70]) data, which can determine not only the primary source parameters but the propagation parameters as well (see for e.g., Korsmeier and Cuoco [39]). We use the CREAM data as the supplement of the AMS-02 data, because it is more compatible with the AMS-02 data when $R \gtrsim 1\,\mathrm{TeV}$.

In this step (Step I), the data set is

$$D_1 = \{D_{\mathrm{p}}^{\text{AMS-02}}, D_{\mathrm{He}}^{\text{AMS-02}}, D_{\bar{\mathrm{p}}/\mathrm{p}}^{\text{AMS-02}}, D_{\mathrm{p}}^{\text{CREAM}}, D_{\mathrm{He}}^{\text{CREAM}}\}\,, \tag{17}$$

and the parameter set is

$$\begin{aligned}\boldsymbol{\theta} =&\{D_0, \delta, z_h, v_A, |N_{\mathrm{p}}, R_{\mathrm{p1}}, R_{\mathrm{p2}}, \nu_{\mathrm{p1}}, \nu_{\mathrm{p2}}, \nu_{\mathrm{p3}}, R_{\mathrm{He1}},\\ &R_{\mathrm{He2}}, \nu_{\mathrm{He1}}, \nu_{\mathrm{He2}}, \nu_{\mathrm{He3}}, |c_{\bar{\mathrm{p}}}, c_{\mathrm{He}}, \phi_{\mathrm{nuc}}, \phi_{\bar{\mathrm{p}}}\}\,.\end{aligned}$$

When the nuclei (proton and helium) primary source and propagation parameters have been determined, we use the best fitting parameters to reproduce the lepton data ($e^- + e^+$, from DAMPE [2]) and the positron data (from AMS-02 [14]). Although there are some systematics between the DAMPE and AMS-02 result, the employed parameter c_{e^+} could reconcile this inconsistence.

In this step (Step II), the data set is

$$D_2 = \{D_{e^+}^{\text{AMS-02}}, D_{e^-+e^+}^{\text{DAMPE}}\}\,. \tag{18}$$

The parameter sets are

$$\begin{aligned}\boldsymbol{\theta}_{\mathrm{psr}} =&\{N_{\mathrm{e}}, R_{\mathrm{e1}}\nu_{\mathrm{e1}}, \nu_{\mathrm{e2}}, |\\ &N_{\mathrm{psr}}, \nu_{\mathrm{psr}}, R_c, |\\ &c_{e^+}, \phi_{e^+}\}\,,\end{aligned}$$

for the excess caused by pulsar and

$$\begin{aligned}\boldsymbol{\theta}_{\mathrm{DM}} =&\{N_{\mathrm{e}}, R_{\mathrm{e1}}\nu_{\mathrm{e1}}, \nu_{\mathrm{e2}}, |\\ &m_\chi, \langle\sigma v\rangle, \eta_e, \eta_\mu, \eta_\tau, |\\ &c_{e^+}, \phi_{e^+}\}\,,\end{aligned}$$

for the excess caused by DM annihilation.

IV. FITTING RESULTS AND DISCUSSION

A. Nuclei fitting results (Step I)

The MCMC algorithm was used to determine the parameters of the Step I as described in Sec. III through fitting to the data set. When the Markov Chains have reached their equilibrium state we take the samples of the parameters as their posterior PDFs. The best-fitting results and the corresponding residuals of the spectra and ratios are showed in Fig. 1. The best-fit values, statistical mean values, standard deviations and allowed intervals at 95% CL for these parameters are shown in Table I.

In Fig. 1, we can see that the nuclei data is perfectly reproduced, which would provide a good precondition for the subsequent fitting on the lepton data. The proton and helium particles $\gtrsim$ TeV would produce the secondary particles (including $\bar{\mathrm{p}}$s and positrons) in lower energy range. Although the CREAM proton and helium data in $\gtrsim$ TeV has a relative large uncertainties, the spectral hardening at $\sim 300\,\mathrm{GeV}$ is accounted and then its influence on secondary products is included.

B. Lepton fitting results (Step II)

The best-fitting results and the corresponding residuals of the lepton and positron spectra are showed in Fig. 2. The corresponding best-fit values, statistical mean values, standard deviations and allowed intervals at 95% CL for these parameters are shown in Table II and Table III.

In Fig. 2, the lepton data can be fitted within uncertainties except the line spectral signal from DAMPE $e^- + e^+$ data at $\sim 1.4\,\mathrm{TeV}$. Although we got small reduced χ^2 from the global fitting in pulsar scenario, if we subtract the line spectral signal ($\sim 1.4\,\mathrm{TeV}$) from DAMPE data and consider the DAMPE data alone, we got $\chi^2 = 22.31$ for pulsar scenario and $\chi^2 = 14.63$ for DM scenario. This result shows (i) the line spectral signal from DAMPE is remarkable for global fitting; (ii) both of these scenarios can not reproduce this signal; (iii) if we subtract this signal, DM scenario gives a better fitting.

In Table II, the value $\nu_{\mathrm{psr}} = 0.68$ is obviously lower than the usual pulsar models [19, 71]. This should be noted for further research.

In Table III, we can see that the DAMPE smooth data constrain m_χ and $\langle\sigma v\rangle$ effectively. It gives a dark matter particle's mass $m_\chi \sim 1280\,\mathrm{GeV}$ and a cross section $\langle\sigma v\rangle \sim 1.48\times10^{-23}\,\mathrm{cm^3\,s^{-1}}$, which also need a suppress factor ($\sim 10^3$) to meet the value $\langle\sigma v\rangle \sim 3\times10^{-26}\,\mathrm{cm^3\,s^{-1}}$ from cosmology [72].

Another interesting property from the DM scenario is the leptonic branching channel of DM annihilation via $\tau\bar{\tau}$ is strongly suppressed, which is obviously different from the fitting results from AMS-02 lepton data.

V. TWO SIMPLE MODELS

We shall propose two simple models to explain the DAMPE results. In these models, we introduce an SM singlet scalar S with quantum number $(\mathbf{1}, \mathbf{1}, \mathbf{0})$ under

ID	Prior range	Best-fit value	Posterior mean and Standard deviation	Posterior 95% range
D_0 (10^{28} cm^2 s^{-1})	[1, 20]	15.51	15.38±0.91	[13.05, 17.15]
δ	[0.1, 1.0]	0.363	0.343±0.031	[0.332, 0.410]
z_h (kpc)	[0.5, 30.0]	25.87	27.01±1.99	[20.78, 29.32]
v_A (km/s)	[0, 80]	49.01	45.30±2.86	[42.86, 52.62]
N_p [a]	[1, 8]	4.48	4.47±0.02	[4.432, 4.498]
$R_{\rm p1}$ (GV)	[1, 30]	26.8	24.52±1.80	[22.51, 29.08]
$R_{\rm p2}$ (GV)	[60, 1000]	536.8	488.36±61.63	[403.46, 690.66]
$\nu_{\rm p1}$	[1.0, 4.0]	2.108	2.155±0.063	[2.019, 2.160]
$\nu_{\rm p2}$	[1.0, 4.0]	2.420	2.444±0.029	[2.381, 2.450]
$\nu_{\rm p3}$	[1.0, 4.0]	2.315	2.408±0.033	[2.240, 2.324]
$R_{\rm He1}$ (GV)	[1, 30]	11.70	11.38±0.54	[10.40, 12.75]
$R_{\rm He2}$ (GV)	[60, 1000]	223.94	246.756±29.462	[204.78, 317.67]
$\nu_{\rm He1}$	[1.0, 4.0]	2.099	2.144±0.055	[2.023, 2.149]
$\nu_{\rm He2}$	[1.0, 4.0]	2.370	2.397±0.033	[2.328, 2.399]
$\nu_{\rm He3}$	[1.0, 4.0]	2.186	2.193±0.036	[2.113, 2.211]
$\phi_{\rm nuc}$ (GV)	[0, 1.5]	0.67	0.73±0.05	[0.61, 0.73]
$\phi_{\bar{\rm p}}$ (GV)	[0, 1.5]	0.48	0.41±0.14	[0.32, 0.75]
$c_{\rm He}$	[0.1, 10.0]	4.468	3.90±0.41	[3.49, 4.94]
$c_{\bar{\rm p}}$	[0.1, 10.0]	1.681	1.60±0.14	[1.45, 1.97]

[a] Post-propagated normalization flux of protons at 100 GeV in unit $10^{-2}\,{\rm m}^{-2}\,{\rm s}^{-1}\,{\rm sr}^{-1}\,{\rm GeV}^{-1}$

TABLE I: Constraints on the propagation models from the global Bayesian analyses to the AMS-02 data of proton flux, helium flux and $\bar{\rm p}$/p ratio. The prior interval, best-fit value, statistic mean, standard deviation and the allowed range at 95% CL are listed for each propagation parameter.

ID	Prior range	Best-fit value	Posterior mean and Standard deviation	Posterior 95% range
$\log(N_{\rm e})$ [a]	[-4, 0]	-1.9356	-1.944±0.007	[-1.960, -1.931]
$\log(R_{\rm e}/{\rm GV})$	[0, 3]	1.6510	1.62±0.03	[1.54, 1.73]
$\nu_{\rm e1}$	[1.0, 4.0]	2.5819	2.51±0.06	[2.34, 2.63]
$\nu_{\rm e2}$	[1.0, 4.0]	2.3826	2.38±0.02	[2.37, 2.42]
$\log(N_{\rm psr})$ [b]	[-8, -4]	-6.1214	-6.144±0.002	[-6.179, -6.099]
$\nu_{\rm psr}$	[0, 3.0]	0.6751	0.72±0.06	[0.54, 0.80]
$\log(R_c/{\rm GV}))$	[2, 5]	2.8193	2.87±0.04	[2.75, 2.92]
ϕ_{e^+} (GV)	[0, 1.5]	1.3698	1.32±0.02	[1.29, 1.39]
c_{e^+}	[0.1, 10.0]	5.0932	5.11±0.07	[5.00, 5.30]

[a] Post-propagated normalization flux of electrons at 25 GeV in unit ${\rm m}^{-2}\,{\rm s}^{-1}\,{\rm sr}^{-1}\,{\rm GeV}^{-1}$
[b] Post-propagated normalization flux of electrons at 300 GeV in unit ${\rm m}^{-2}\,{\rm s}^{-1}\,{\rm sr}^{-1}\,{\rm GeV}^{-1}$

TABLE II: Constraints on the parameters to reproduce the lepton data from DAMPE and AMS-02 via global Bayesian analyses of pulsar scenario. The prior interval, best-fit value, statistic mean, standard deviation and the allowed range at 95% CL are listed for each propagation parameter.

$SU(3)_C \times SU(2)_L \times U(1)_Y$ gauge symmetry. We assume that S is odd under a discrete Z_2 symmetry and then a dark matter candidate.

In Model I, we introduce a doublet scalar H' with quantum numbers $(\mathbf{1}, \mathbf{2}, -\mathbf{1/2})$. We assume that$H'$ couples dominantly to the charged leptons, and does not have a VEV or has a very small VEV. The relevant new Lagrangian is given as follows

$$\begin{aligned} -\mathcal{L} = & m_S^2|S|^2 + m_{H'}^2|H'|^2 + \lambda_S|S|^4 + \lambda_{H'}|H'|^4 \\ & + \lambda_{SH'}|S|^4|H'|^2 + \lambda_{SH}|S|^4|H|^2 + \lambda_{H'H}|H'|^4|H|^2 \\ & + \Big(\lambda_{SHH'}|S|^2\tilde{H}H' + y^e_{ij}L_iE^c_jH' + y^u_{ij}Q_iU^c_j\tilde{H}' \\ & + y^d_{ij}Q_iD^c_jH' + {\rm H.C.}\Big) \ , \end{aligned} \tag{19}$$

where $\tilde{H} = i\sigma_2 H^*$, and $\tilde{H}' = i\sigma_2 H'^*$, as well as Q_i, U^c_i, D^c_i, L_i, E^c_i are the left-handed quark doublets, right-handed up-type quarks, right-handed down-type quarks, left-handed lepton doublets, right-handed charged lep-

ID	Prior range	Best-fit value	Posterior mean and Standard deviation	Posterior 95% range
$\log(N_{\rm e})$ [a]	[-4, 0]	-1.940	-1.943±0.007	[-1.958, -1.928]
$\log(R_{\rm e}/\,{\rm GV})$	[0, 3]	1.61985	1.626±0.037	[1.57, 1.74]
$\nu_{\rm e1}$	[1.0, 4.0]	2.5548	2.54±0.03	[2.46, 2.60]
$\nu_{\rm e2}$	[1.0, 4.0]	2.3704	2.37±0.01	[2.34, 2.40]
$\log(m_\chi/\,{\rm GeV})$	[1, 6]	3.0822	3.085±0.006	[3.076, 3.096]
$\log(\langle\sigma v\rangle)$ [b]	[-28, -18]	-22.83	-22.80±0.06	[-22.93, -22.70]
η_e	[0, 1]	0.484	0.479±0.007	[0.466, 0.488]
η_μ	[0, 1]	0.508	0.508±0.008	[0.493, 0.518]
η_τ	[0, 1]	0.008	0.013±0.010	[0.001, 0.032]
ϕ_{e^+} (GV)	[0, 1.5]	1.315	1.314±0.009	[1.296, 1.332]
c_{e^+}	[0.1, 10.0]	5.02	5.03±0.03	[4.97, 5.08]

[a] Post-propagated normalization flux of electrons at 25 GeV in unit $\rm m^{-2}\,s^{-1}\,sr^{-1}\,GeV^{-1}$
[b] In unit $\rm cm^3 s^{-1}$

TABLE III: The same as Tab. II, but for DM scenario.

tons, respectively. For simplicity, we assume that H' couples dominantly to the charged leptons, *i.e.*, $y^e_{ij} >> y^u_{ij}/y^d_{ij}$. After the electroweak symmetry breaking, we obtain $\lambda_{SHH'}\langle\tilde{H}\rangle|S|^2H'$, and then the dark matter particles can annihilate dominantly into charged leptons.

In Model II, we introduce a pair of vector-like fermions (XE, XE^c), which are odd under Z_2 symmetry as well. The quantum numbers for XE and XE^c are $(\mathbf{1},\mathbf{1},-\mathbf{1})$ and $(\mathbf{1},\mathbf{1},\mathbf{1})$, respectively. The relevant new Lagrangian is given as follows

$$-\mathcal{L} = m_S^2|S|^2 + \lambda_S|S|^4 + +\lambda_{SH}|S|^4|H|^2 + \\ + (y^e_i E^c_i XES + M_{XE}XE^cXE + \text{H.C.}) \ , \quad (20)$$

Thus, the dark matter particles can annihilate into charged leptons via t and u channels.

Before closing this section, we would like to give some comment on the tentative spectral peak at 1.4 TeV presented in DAMPE data. Since cooling process of high energy cosmic-ray electrons in the Galactic halo will effectively smooth out the spectral features, such sharp peak indicates there may exist a nearby electron source [78]. Both astrophysical sources (e.g., pulsars) and DM interpretations are discussed in Yuan et al. [78]. For the DM interpretation, they found that a DM particle with standard WIMP annihilation cross section $3\times10^{-26}{\rm cm}^3 s^{-1}$ and annihilate into $e^\pm$ or $e^\pm$, $\mu^\pm$, $\tau^\pm$ with $1:1:1$ ratio could well fit the peak if introducing a nearby DM subhalo located at 0.1-0.3 kpc (1 kpc) away from the solar system for DM mass of 1.5 (2.2) TeV [78]. Obviously, our model is also suitable to explain such spectral peak in DAMPE data since all of above requirements are easy to satisfy with appropriate assumption of nearby subhalo.

VI. CONCLUSION

In this work, we did Bayesian analysis on the newly released CREs data from DAMPE to study the extra source properties in it. In order to deduct the primary electrons and the secondary in CREs flux consistently and precisely, we separate our global fitting into 2 steps. In Step I, we reproduce the proton flux, helium flux and $\bar{\rm p}/{\rm p}$ ratio to determine the propagation and primary source parameters. In Step II, we used the best fit parameters in Step I and did global fitting to the CREs flux from DAMPE and positron flux from AMS-02. Two independent scenarios are considered in Step II, which account the extra source for pulsars and DM annihilation (via leptonic channels).

The line spectral signal at 1.4 TeV shows a significant influence on the global fitting level. If we include this signal, the global fitting result favors a pulsar scenario. If we deduct this signal, the DM scenario gives a much better fitting level. But neither of the scenarios can fit this signal properly. Some of the solutions of this problem is to employ nearby pulsars wind, DM clumps, and supernova remnants [19, 71, 73–78]. On the other hand, considering the statistical confidence level of this signal is about 3σ, more events should be accumulated in future.

In the DM scenario, the fitting result gives a dark matter particle's mass $m_\chi \sim 1280\,{\rm GeV}$ and a cross section $\langle\sigma v\rangle \sim 1.48\times10^{-23}\,{\rm cm}^3\,{\rm s}^{-1}$. This is benefited from the break at $\sim 1\,{\rm TeV}$. In such configurations, the cross section in this work still should have a suppress factor to meet the value $\langle\sigma v\rangle \sim 3\times10^{-26}\,{\rm cm}^3\,{\rm s}^{-1}$. Moreover, the $\tau\bar{\tau}$ annihilation channel is strongly suppressed. The e^-e^+ and $\mu\bar{\mu}$ channels are almost equally weighted.

Furthermore, we proposed two simple models to explain the DAMPE results. We introduce an SM singlet dark matter scalar S in these models. In Model I, we introduced a doublet scalar H' without a VEV or with a very small VEV. And H' couples dominantly to the charged leptons. With the term S^2HH', the dark matter particles can annihilate dominantly into charged leptons via s channel after electroweak symmetry breaking. In Model II, we introduced a pair of vector-like fermions (XE, XE^c), and the dark matter particles can annihilate

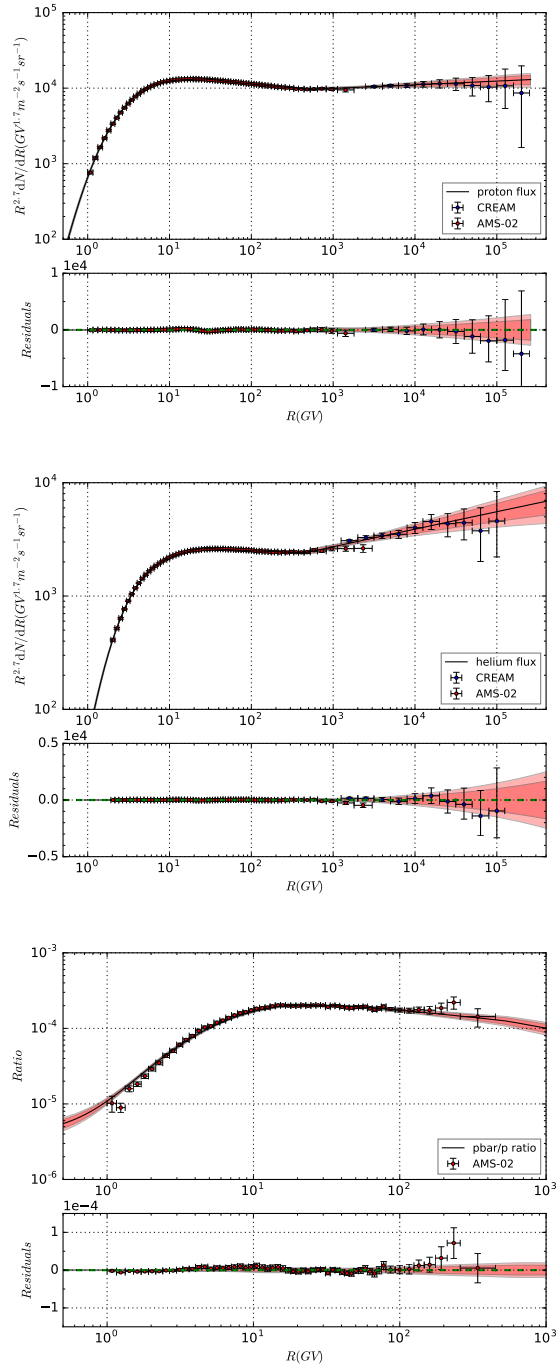

FIG. 1: The global fitting results and the corresponding residuals to the AMS-02 proton flux, helium flux and $\bar{\mathrm{p}}/\mathrm{p}$ ratio. The 2σ (deep red) and 3σ (light red) bound are also showed in the figures. For best-fit result, $\chi^2/d.o.f. = 153.52/198$

into charged leptons via t and u channels.

Note: During the preparation of our paper, we noticed the several papers, Fan et al. [79], Duan et al. [80], Gu and He [81] , which all considered the $U(1)'$ models. Thus, our two simple models are different from these studies.

ACKNOWLEDGMENTS

We would like to thank Maurin et al. [82] to collect database and associated online tools for charged cosmic-ray measurements. This research was supported in part by the Projects 11475238 and 11647601 supported by National Science Foundation of China, and by Key Research Program of Frontier Sciences, CAS. The calculation in this paper are supported by HPC Cluster of SKLTP/ITP-CAS.

[1] C. Jin, Chinese Journal of Space Science **34**, 550 (2014).
[2] DAMPE Collaboration, Nature **294**, L41 (2017).
[3] O. Adriani, G. C. Barbarino, G. A. Bazilevskaya, R. Bellotti, M. Boezio, E. A. Bogomolov, L. Bonechi, M. Bongi,

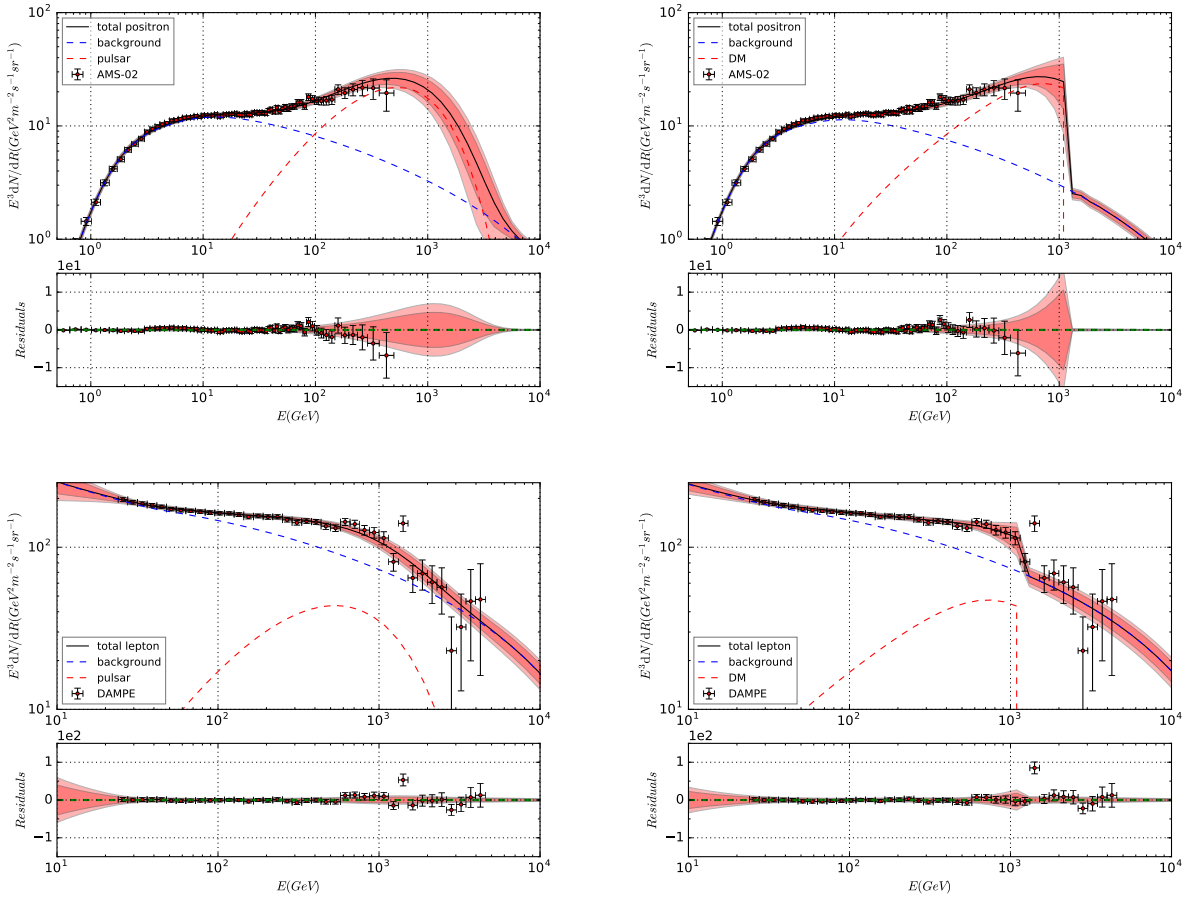

FIG. 2: The global fitting results and the corresponding residuals to the AMS-02 positron flux and DAMPE lepton flux. The 2σ (deep red) and 3σ (light red) bound are also showed in the figures. The first column shows the fitting results of pulsar and the second shows the fitting results of DM. In Step II, χ^2/d.o.f = 86.61/101 for pulsar scenario and χ^2/d.o.f = 109.59/99 for DM scenario.

V. Bonvicini, S. Bottai, and et al., Nature **458**, 607 (2009), arXiv:0810.4995.

[4] PAMELA Collaboration, O. Adriani, G. C. Barbarino, G. A. Bazilevskaya, R. Bellotti, M. Boezio, E. A. Bogomolov, L. Bonechi, M. Bongi, V. Bonvicini, S. Borisov, and el al., Astroparticle Physics **34**, 1 (2010), arXiv:1001.3522 [astro-ph.HE].

[5] AMS Collaboration, M. Aguilar, D. Aisa, B. Alpat, A. Alvino, G. Ambrosi, K. Andeen, L. Arruda, N. Attig, P. Azzarello, A. Bachlechner, and et al., Physical Review Letters **113**, 221102 (2014).

[6] Fermi-LAT Collaboration, M. Ackermann, M. Ajello, A. Allafort, W. B. Atwood, L. Baldini, G. Barbiellini, D. Bastieri, K. Bechtol, R. Bellazzini, B. Berenji, and el al., Physical Review Letters **108**, 011103 (2012), arXiv:1109.0521 [astro-ph.HE].

[7] C. Collaboration, O. Adriani, Y. Akaike, K. Asano, Y. Asaoka, M. G. Bagliesi, G. Bigongiari, W. R. Binns, S. Bonechi, M. Bongi, P. Brogi, and et al. (CALET Collaboration), Phys. Rev. Lett. **119**, 181101 (2017).

[8] F.-L. Collaboration, S. Abdollahi, M. Ackermann, M. Ajello, W. B. Atwood, L. Baldini, G. Barbiellini, D. Bastieri, R. Bellazzini, E. D. Bloom, and et al. (The Fermi-LAT Collaboration), Phys. Rev. D **95**, 082007 (2017).

[9] AMS Collaboration, M. Aguilar, G. Alberti, B. Alpat, A. Alvino, G. Ambrosi, K. Andeen, H. Anderhub, L. Arruda, P. Azzarello, A. Bachlechner, and et al., Physical Review Letters **110**, 141102 (2013).

[10] S. W. Barwick, J. J. Beatty, A. Bhattacharyya, C. R. Bower, C. J. Chaput, S. Coutu, G. A. de Nolfo, J. Knapp, D. M. Lowder, S. McKee, D. Mueller, J. A. Musser, S. L. Nutter, E. Schneider, S. P. Swordy, G. Tarle, A. D. Tomasch, E. Torbet, and HEAT Collaboration, Astrophys. J. Lett. **482**, L191 (1997), astro-ph/9703192.

[11] AMS-01 Collaboration, Physics Letters B **646**, 145 (2007), astro-ph/0703154.

[12] AMS Collaboration, M. Aguilar, G. Alberti, B. Alpat, A. Alvino, G. Ambrosi, K. Andeen, H. Anderhub, L. Arruda, P. Azzarello, A. Bachlechner, and et al., Physical Review Letters **110**, 141102 (2013).

[13] AMS Collaboration, L. Accardo, M. Aguilar, D. Aisa, A. Alvino, G. Ambrosi, K. Andeen, L. Arruda, N. Attig, P. Azzarello, A. Bachlechner, and et al., Physical Review Letters **113**, 121101 (2014).

[14] AMS Collaboration, M. Aguilar, D. Aisa, A. Alvino, G. Ambrosi, K. Andeen, L. Arruda, N. Attig, P. Azzarello, A. Bachlechner, F. Barao, and et al., Physical Review Letters **113**, 121102 (2014).

[15] C. S. Shen, Astrophys. J. Lett. **162**, L181 (1970).

[16] L. Zhang and K. S. Cheng, Astron. Astrophys. **368**, 1063 (2001).

[17] H. Yüksel, M. D. Kistler, and T. Stanev, Physical Review Letters **103**, 051101 (2009), arXiv:0810.2784.

[18] D. Hooper, P. Blasi, and P. Dario Serpico, J. Cosmol. Astropart. Phys. **1**, 025 (2009), arXiv:0810.1527.

[19] S. Profumo, Central European Journal of Physics **10**, 1 (2012), arXiv:0812.4457.

[20] P. Blasi, Physical Review Letters **103**, 051104 (2009), arXiv:0903.2794 [astro-ph.HE].

[21] H.-B. Hu, Q. Yuan, B. Wang, C. Fan, J.-L. Zhang, and X.-J. Bi, Astrophys. J. Lett. **700**, L170 (2009), arXiv:0901.1520 [astro-ph.HE].

[22] Y. Fujita, K. Kohri, R. Yamazaki, and K. Ioka, Phys. Rev. D **80**, 063003 (2009), arXiv:0903.5298 [astro-ph.HE].

[23] L. Bergström, T. Bringmann, and J. Edsjö, Phys. Rev. D **78**, 103520 (2008), arXiv:0808.3725.

[24] V. Barger, W.-Y. Keung, D. Marfatia, and G. Shaughnessy, Physics Letters B **672**, 141 (2009), arXiv:0809.0162 [hep-ph].

[25] M. Cirelli, M. Kadastik, M. Raidal, and A. Strumia, Nuclear Physics B **813**, 1 (2009), arXiv:0809.2409 [hep-ph].

[26] J. Zhang, X.-J. Bi, J. Liu, S.-M. Liu, P.-F. Yin, Q. Yuan, and S.-H. Zhu, Phys. Rev. D **80**, 023007 (2009), arXiv:0812.0522.

[27] L. Bergström, J. Edsjö, and G. Zaharijas, Physical Review Letters **103**, 031103 (2009), arXiv:0905.0333 [astro-ph.HE].

[28] P.-F. Yin, Z.-H. Yu, Q. Yuan, and X.-J. Bi, Phys. Rev. D **88**, 023001 (2013), arXiv:1304.4128 [astro-ph.HE].

[29] A. Lewis and S. Bridle, Phys. Rev. D **66**, 103511 (2002), astro-ph/0205436.

[30] J. Liu, Q. Yuan, X. Bi, H. Li, and X. Zhang, Phys. Rev. D **81**, 023516 (2010), arXiv:0906.3858 [astro-ph.CO].

[31] S.-J. Lin, Q. Yuan, and X.-J. Bi, Physical Review D **91**, 063508 (2015), arXiv:1409.6248 [astro-ph.HE].

[32] Q. Yuan, S.-J. Lin, K. Fang, and X.-J. Bi, ArXiv e-prints (2017), arXiv:1701.06149 [astro-ph.HE].

[33] J.-S. Niu and T. Li, ArXiv e-prints (2017), arXiv:1705.11089 [astro-ph.HE].

[34] A. D. Panov, J. H. Adams, H. S. Ahn, G. L. Bashindzhagyan, K. E. Batkov, J. Chang, M. Christl, A. R. Fazely, O. Ganel, R. M. Gunashingha, T. G. Guzik, J. Isbert, K. C. Kim, E. N. Kouznetsov, M. I. Panasyuk, W. K. H. Schmidt, E. S. Seo, N. V. Sokolskaya, J. W. Watts, J. P. Wefel, J. Wu, and V. I. Zatsepin, ArXiv Astrophysics e-prints (2006), astro-ph/0612377.

[35] H. S. Ahn, P. Allison, M. G. Bagliesi, J. J. Beatty, G. Bigongiari, J. T. Childers, N. B. Conklin, S. Coutu, M. A. DuVernois, O. Ganel, J. H. Han, J. A. Jeon, K. C. Kim, M. H. Lee, L. Lutz, P. Maestro, A. Malinin, P. S. Marrocchesi, S. Minnick, S. I. Mognet, J. Nam, S. Nam, S. L. Nutter, I. H. Park, N. H. Park, E. S. Seo, R. Sina, J. Wu, J. Yang, Y. S. Yoon, R. Zei, and S. Y. Zinn, Astrophys. J. Lett. **714**, L89 (2010), arXiv:1004.1123 [astro-ph.HE].

[36] PAMELA Collaboration, O. Adriani, G. C. Barbarino, G. A. Bazilevskaya, R. Bellotti, M. Boezio, E. A. Bogomolov, L. Bonechi, M. Bongi, V. Bonvicini, S. Borisov, and el al., Science **332**, 69 (2011), arXiv:1103.4055 [astro-ph.HE].

[37] AMS Collaboration, M. Aguilar, D. Aisa, B. Alpat, A. Alvino, G. Ambrosi, K. Andeen, L. Arruda, N. Attig, P. Azzarello, A. Bachlechner, and et al., Physical Review Letters **114**, 171103 (2015).

[38] AMS Collaboration, M. Aguilar, D. Aisa, B. Alpat, A. Alvino, G. Ambrosi, K. Andeen, L. Arruda, N. Attig, P. Azzarello, A. Bachlechner, and et al., Physical Review Letters **115**, 211101 (2015).

[39] M. Korsmeier and A. Cuoco, ArXiv e-prints (2016), arXiv:1607.06093 [astro-ph.HE].

[40] A. W. Strong, I. V. Moskalenko, and V. S. Ptuskin, Annual Review of Nuclear and Particle Science **57**, 285 (2007), astro-ph/0701517.

[41] E. S. Seo and V. S. Ptuskin, Astrophys. J. **431**, 705 (1994).

[42] A. W. Strong, I. V. Moskalenko, and O. Reimer, Astrophys. J. **537**, 763 (2000), astro-ph/9811296.

[43] PAMELA Collaboration, O. Adriani, G. C. Barbarino, G. A. Bazilevskaya, R. Bellotti, M. Boezio, E. A. Bogomolov, L. Bonechi, M. Bongi, V. Bonvicini, S. Borisov, and el al., Science **332**, 69 (2011), arXiv:1103.4055 [astro-ph.HE].

[44] G. Case and D. Bhattacharya, American Association of Pharmaceutical Scientists **120**, 437 (1996).

[45] A. W. Strong and I. V. Moskalenko, Astrophys. J. **509**, 212 (1998), astro-ph/9807150.

[46] R. Trotta, G. Jóhannesson, I. V. Moskalenko, T. A. Porter, R. Ruiz de Austri, and A. W. Strong, Astrophys. J. **729**, 106 (2011), arXiv:1011.0037 [astro-ph.HE].

[47] Fermi-LAT Collaboration, L. Tibaldo, and I. A. Grenier, ArXiv e-prints (2009), arXiv:0907.0312 [astro-ph.HE].

[48] L. C. Tan and L. K. Ng, Journal of Physics G Nuclear Physics **9**, 1289 (1983).

[49] R. P. Duperray, C.-Y. Huang, K. V. Protasov, and M. Buénerd, Phys. Rev. D **68**, 094017 (2003), astro-ph/0305274.

[50] R. Kappl and M. W. Winkler, J. Cosmol. Astropart. Phys. **9**, 051 (2014), arXiv:1408.0299 [hep-ph].

[51] M. di Mauro, F. Donato, A. Goudelis, and P. D. Serpico, Phys. Rev. D **90**, 085017 (2014), arXiv:1408.0288 [hep-ph].

[52] T. Delahaye, R. Lineros, F. Donato, N. Fornengo, J. Lavalle, P. Salati, and R. Taillet, Astron. Astrophys. **501**, 821 (2009), arXiv:0809.5268.

[53] M. Mori, Astroparticle Physics **31**, 341 (2009), arXiv:0903.3260 [astro-ph.HE].

[54] M. Cirelli, G. Corcella, A. Hektor, G. Hütsi, M. Kadastik, P. Panci, M. Raidal, F. Sala, and A. Strumia, J. Cosmol. Astropart. Phys. **3**, 051 (2011), arXiv:1012.4515 [hep-ph].

[55] P. Ciafaloni, D. Comelli, A. Riotto, F. Sala, A. Strumia, and A. Urbano, J. Cosmol. Astropart. Phys. **3**, 019 (2011), arXiv:1009.0224 [hep-ph].

[56] J. F. Navarro, E. Hayashi, C. Power, A. R. Jenkins, C. S. Frenk, S. D. M. White, V. Springel, J. Stadel, and T. R. Quinn, Mon. Not. Roy. Astron. Soc. **349**, 1039 (2004), astro-ph/0311231.

[57] D. Merritt, A. W. Graham, B. Moore, J. Diemand, and B. Terzić, Astron. J. **132**, 2685 (2006), astro-

ph/0509417.
[58] J. Einasto, ArXiv e-prints (2009), arXiv:0901.0632 [astro-ph.CO].
[59] J. F. Navarro, A. Ludlow, V. Springel, J. Wang, M. Vogelsberger, S. D. M. White, A. Jenkins, C. S. Frenk, and A. Helmi, Mon. Not. Roy. Astron. Soc. **402**, 21 (2010), arXiv:0810.1522.
[60] R. Catena and P. Ullio, J. Cosmol. Astropart. Phys. **8**, 004 (2010), arXiv:0907.0018.
[61] M. Weber and W. de Boer, Astron. Astrophys. **509**, A25 (2010), arXiv:0910.4272 [astro-ph.CO].
[62] P. Salucci, F. Nesti, G. Gentile, and C. Frigerio Martins, Astron. Astrophys. **523**, A83 (2010), arXiv:1003.3101.
[63] M. Pato, O. Agertz, G. Bertone, B. Moore, and R. Teyssier, Phys. Rev. D **82**, 023531 (2010), arXiv:1006.1322 [astro-ph.HE].
[64] F. Iocco, M. Pato, G. Bertone, and P. Jetzer, J. Cosmol. Astropart. Phys. **11**, 029 (2011), arXiv:1107.5810 [astro-ph.GA].
[65] L. J. Gleeson and W. I. Axford, Astrophys. J. **154**, 1011 (1968).
[66] C. Evoli, D. Gaggero, D. Grasso, and L. Maccione, J. Cosmol. Astropart. Phys. **10**, 018 (2008), arXiv:0807.4730.
[67] G. Jóhannesson, R. Ruiz de Austri, A. C. Vincent, I. V. Moskalenko, E. Orlando, T. A. Porter, A. W. Strong, R. Trotta, F. Feroz, P. Graff, and M. P. Hobson, Astrophys. J. **824**, 16 (2016), arXiv:1602.02243 [astro-ph.HE].
[68] J. Goodman and J. Weare, Communications in Applied Mathematics and Computational Science **5**, 65 (2010).
[69] D. Foreman-Mackey, D. W. Hogg, D. Lang, and J. Goodman, Publications of the Astronomical Society of the Pacific **125**, 306 (2013), arXiv:1202.3665 [astro-ph.IM].
[70] AMS Collaboration, M. Aguilar, L. Ali Cavasonza, B. Alpat, G. Ambrosi, L. Arruda, N. Attig, S. Aupetit, P. Azzarello, A. Bachlechner, F. Barao, and et al., Physical Review Letters **117**, 091103 (2016).
[71] A. D. Panov, in Journal of Physics Conference Series, Journal of Physics Conference Series, Vol. 409 (2013) p. 012004, arXiv:1303.6118 [astro-ph.HE].
[72] G. Jungman, M. Kamionkowski, and K. Griest, Phys. Rept. **267**, 195 (1996), hep-ph/9506380.
[73] D. Malyshev, I. Cholis, and J. Gelfand, Phys. Rev. D **80**, 063005 (2009), arXiv:0903.1310 [astro-ph.HE].
[74] M. Kuhlen and D. Malyshev, Phys. Rev. D **79**, 123517 (2009), arXiv:0904.3378 [hep-ph].
[75] P. Brun, T. Delahaye, J. Diemand, S. Profumo, and P. Salati, Phys. Rev. D **80**, 035023 (2009), arXiv:0904.0812 [astro-ph.HE].
[76] L. Gendelev, S. Profumo, and M. Dormody, J. Cosmol. Astropart. Phys. **2**, 016 (2010), arXiv:1001.4540 [astro-ph.HE].
[77] K. Fang, X.-J. Bi, and P.-F. Yin, ArXiv e-prints (2017), arXiv:1711.10996 [astro-ph.HE].
[78] Q. Yuan, L. Feng, P.-F. Yin, Y.-Z. Fan, X.-J. Bi, M.-Y. Cui, T.-K. Dong, Y.-Q. Guo, K. Fang, H.-B. Hu, X. Huang, S.-J. Lei, X. Li, S.-J. Lin, H. Liu, P.-X. Ma, W.-X. Peng, R. Qiao, Z.-Q. Shen, M. Su, Y.-F. Wei, Z.-L. Xu, C. Yue, J.-J. Zang, C. Zhang, X. Zhang, Y.-P. Zhang, Y.-J. Zhang, and Y.-L. Zhang, ArXiv e-prints (2017), arXiv:1711.10989 [astro-ph.HE].
[79] Y.-Z. Fan, W.-C. Huang, M. Spinrath, Y.-L. Sming Tsai, and Q. Yuan, ArXiv e-prints (2017), arXiv:1711.10995 [hep-ph].
[80] G. H. Duan, L. Feng, F. Wang, L. Wu, J. M. Yang, and R. Zheng, ArXiv e-prints (2017), arXiv:1711.11012 [hep-ph].
[81] P.-H. Gu and X.-G. He, ArXiv e-prints (2017), arXiv:1711.11000 [hep-ph].
[82] D. Maurin, F. Melot, and R. Taillet, Astron. Astrophys. **569**, A32 (2014), arXiv:1302.5525 [astro-ph.HE].